

Cloud top altitude
and geometrical
thickness study

G. Merlin et al.

This discussion paper is/has been under review for the journal Atmospheric Measurement Techniques (AMT). Please refer to the corresponding final paper in AMT if available.

Cloud information content analysis of multi-angular measurements in the oxygen A-band: application to 3MI and MSPI

G. Merlin¹, J. Riedi¹, L. C. Labonnote¹, C. Cornet¹, A. B. Davis², P. Dubuisson¹, M. Desmons³, N. Ferlay¹, and F. Parol¹

¹Laboratoire d'Optique Atmosphérique, Université de Lille 1, Sciences et Technologies, Villeneuve d'Ascq, France

²Jet Propulsion Laboratory, California Institute of Technology, Pasadena, CA, USA

³Department of Meteorology, University of Reading, Berkshire, UK

Received: 14 September 2015 – Accepted: 6 November 2015 – Published: 4 December 2015

Correspondence to: G. Merlin (guillaume.merlin@ed.univ-lille1.fr)

Published by Copernicus Publications on behalf of the European Geosciences Union.

Title Page

Abstract

Introduction

Conclusions

References

Tables

Figures



Back

Close

Full Screen / Esc

Printer-friendly Version

Interactive Discussion



Abstract

The vertical distribution of cloud cover has a significant impact on a large number of meteorological and climatic processes. Cloud top altitude and cloud geometrical thickness are then essential. Previous studies established the possibility of retrieving those parameters from multi-angular oxygen A-band measurements. Here we perform a study and comparison of the performances of future instruments. The 3MI (Multi-angle, Multi-channel and Multi-polarization Imager) instrument developed by EUMETSAT, which is an extension of the POLDER/PARASOL instrument, and MSPI (Multi-angles Spectro-Polarimetric Imager) developed by NASA's Jet Propulsion Laboratory will measure total and polarized light reflected by the Earth's atmosphere-surface system in several spectral bands (from UV to SWIR) and several viewing geometries. Those instruments should provide opportunities to observe the links between the cloud structures and the anisotropy of the reflected solar radiation into space. Specific algorithms will need be developed in order to take advantage of the new capabilities of this instrument. However, prior to this effort, we need to understand, through a theoretical Shannon information content analysis, the limits and advantages of these new instruments for retrieving liquid and ice cloud properties, and especially, in this study, the amount of information coming from the A-Band channel on the cloud top altitude (CTOP) and geometrical thickness (CGT). We compare the information content of 3MI A-Band in two configurations and that of MSPI. Quantitative information content estimates show that the retrieval of CTOP with a high accuracy is possible in almost all cases investigated. The retrieval of CGT seems less easy but possible for optically thick clouds above a black surface, at least when $CGT > 1-2$ km.

Cloud top altitude and geometrical thickness study

G. Merlin et al.

Title Page

Abstract

Introduction

Conclusions

References

Tables

Figures



Back

Close

Full Screen / Esc

Printer-friendly Version

Interactive Discussion



ods applied on stereo observations (Moroney et al., 2002; Seiz et al., 2007; Wu et al., 2009).

Information on cloud top location from passive instruments can also be obtained through the exploitation of dioxygen differential absorption of solar radiation in the A-band, as first suggested by Yamamoto and Wark (1961). Indeed, molecular oxygen is a well-mixed atmospheric gas and, consequently, the amount of absorption is linked with the photon geometrical pathlength in the atmosphere, which is limited, at a first order, by the cloud top altitude. However, clouds are not solid (surface-like) reflectors. The additional absorption of radiation occurring along the path inside the cloud leads to significant biases and uncertainties in the retrieved cloud-top pressure, as shown by Preusker and Lindstrot (2009). Some studies have shown, however, that this multiple scattering effect can be used to obtain information on photon path lengths within the clouds, which in turn could inform on cloud geometrical thickness (e.g., Davis et al., 2009, and references therein). Depending on the instruments characteristics in terms of spectral resolution and coverage, multi-angular capabilities, different methods have been proposed or applied. Rozanov and Kokhanovsky (2004) developed a retrieval technique exploiting hyperspectral A-band measurements from SCIAMACHY, thanks to a semi-analytical algorithm using asymptotic theory. The hyperspectral approach to A-band measurement was further evaluated through a recent information content analysis (Schuessler et al., 2014). Turning to narrowband bispectral multi-angular measurements in the A-band, Ferlay et al. (2010) suggested to use the correlation between the angular standard deviation of the cloud oxygen pressure and the cloud geometrical thickness. The feasibility of this technique was, later on, confirmed by Desmons et al. (2013), who compared POLDER3/PARASOL retrievals of cloud geometrical thickness to information derived from collocated active sensors (CALIOP/CLOUDSAT). At the same time, a similar approach was proposed to use the differential absorption occurring between single-view measurements in the O₂ A- and B-bands (Yang et al., 2013).

Most of those studies have been limited to monolayer optically thick clouds over ocean. In addition, except for the study by Schuessler et al. (2014), most previous

Cloud top altitude and geometrical thickness study

G. Merlin et al.

Title Page

Abstract

Introduction

Conclusions

References

Tables

Figures



Back

Close

Full Screen / Esc

Printer-friendly Version

Interactive Discussion



Cloud top altitude and geometrical thickness study

G. Merlin et al.

Title Page

Abstract

Introduction

Conclusions

References

Tables

Figures



Back

Close

Full Screen / Esc

Printer-friendly Version

Interactive Discussion



studies have not formally considered the impact of measurements and forward model errors on the retrievals. Our work aims to develop a comprehensive analysis of the information provided by multi-angle and bispectral measurements in the O₂ A-band to derive the vertical location and extent of clouds (cloud top altitude and cloud geometrical thickness). Building on previous analyses by Ferlay et al. (2010) and Desmons et al. (2013), our present analysis aims at understanding the feasibility of retrieving those parameters for all types of clouds (liquid/ice, thin/thick) and for a range of surface albedo values. This investigation is motivated by the need to develop physics-based algorithms that will be applied globally to measurements from a new generation of multi-angle sensors.

Several studies have demonstrated the great interest of combining multi-spectral, multi-angular and polarized measurements in the visible, near and shortwave infrared to better constrain retrievals of cloud microphysical (Bréon and Doutriaux-Boucher, 2005; Zhang et al., 2009; Riedi et al., 2010) and macrophysical (Ferlay et al., 2010; Desmons et al., 2013) properties. In this context, several missions that will fly a new generation of polarimetric multi-angular sensors that are currently being formulated. Here, we focus on the Multi-viewing, Multi-channel, Multi-polarization Imaging mission (3MI) on the EUMETSAT Polar System-Second generation (EPS-SG) and the Multi-angle Spectro-Polarimetric Imager (MSPI) proposed, among others, for NASA's Aerosol-Cloud-Ecosystem (ACE) mission.

This paper is organized as follows. In Sect. 2, we describe the main characteristics of the 3MI and MSPI instruments that are relevant to our study and describe the simulation scenario performed for each. In Sect. 3, we qualitatively illustrate and discuss the sensitivity of multi-angle A-band measurements to cloud top altitude and geometrical thickness. In Sect. 4, we go further by developing a formal information content analysis of multi-angle O₂ A-band measurements and discuss the impact of various model assumptions and errors on available information. In particular, the cases of dark and bright surfaces are discussed to evaluate the feasibility of a retrieval algorithm that could be applied globally. In Sect. 5, we discuss our results and potential pathways

radiation crosses the entire cloud, paths 3 can be neglected. This explains why previous studies have usually been limited to those thick clouds (Rozanov and Kokhanovsky, 2004; Davis et al., 2009; Ferlay et al., 2010; Yang et al., 2013).

In a first step, we considered the surface as black, which is a good approximation of measurements performed over the ocean. In this case, contribution from path 3 is null. To illustrate in a simple way the sensitivity of measurements to relevant parameters, we represent in Fig. 4 the bands ratio for several top altitudes (CTOP) for three values of COT (1, 4, 16) varying against the air mass factor defined as:

$$m_{\text{air}} = \frac{1}{\cos \theta_v} + \frac{1}{\cos \theta_s} \quad (1)$$

Figure 4 shows O_2 A-band ratio in the solar plane with a solar zenith angle of 30° . The cloud geometrical thickness is fixed at 0.5 km; the cloud droplet size distribution is chosen to be log-normal with an effective radius of $12 \mu\text{m}$ and an effective variance of 0.02. The different colored curves represents different values of CTOP (from 1 to 6 km). For each air mass we obtain two values of the ratio: the upper part correspond to the backscattering direction and the lower to the forward scattering direction.

The two branches of the curves correspond to the forward and backward scattering halves of the principal plane. The latter shows a distinctive angular feature in the near-backscattering direction that is traceable to the phase function and that diminishes as COT increases. Evidently, the A-band ratio decreases generally as the air mass factor hence the absorption increases. A variation of CTOP leads to a variation of path 1 directly (Fig. 3). By increasing CTOP, the photon pathlength above the cloud is decreased. The absorption of the in-band is thus reduced whereas the one of the out-band is not affected by absorption. Consequently, the ratio increases with CTOP, as can be seen in Fig. 4. We note that ratio change due to CTOP variation is almost the same for any angle so no angular signature of CTOP change. Indeed, for optically thick clouds, the band ratio decreases linearly with the air mass, which is the expected behavior when the cloud is assumed to be a solid reflector.

Cloud top altitude and geometrical thickness study

G. Merlin et al.

Title Page

Abstract

Introduction

Conclusions

References

Tables

Figures

◀

▶

◀

▶

Back

Close

Full Screen / Esc

Printer-friendly Version

Interactive Discussion



Cloud top altitude and geometrical thickness study

G. Merlin et al.

Title Page

Abstract

Introduction

Conclusions

References

Tables

Figures



Back

Close

Full Screen / Esc

Printer-friendly Version

Interactive Discussion



Figure 5 is the same as Fig. 4 but with a fixed cloud top altitude (6 km) and for varying geometrical thickness CGT (from 1 to 5 km). It corresponds to a variation of path 2 as the CTOP is constant and the surface black. The ratio decreases as CGT increases. Indeed, for a fixed CTOP and constant COT, an increase of CGT leads to a decrease of the extinction within the cloud. It yields a deeper penetration and an enhanced mean free path of the photon and therefore an increase of absorption in the affected channel and a decrease of the ratio.

For $COT = 1$, we notice differences between forward and backward scattering, which are linked to cloud particle microphysics through their phase function asymmetry factor. The photon pathlength is, in case of low COT, longer in the forward view direction and so larger is the absorption. This effect is more pronounced when CGT increases because, for a fixed COT the extinction within the cloud decreases leading to a deeper the penetration inside the cloud. Variations of the ratio due to CGT changes are thus significantly angularly dependent for this case of an optically thin cloud. Thus, as can be seen on Figs. 4 and 5, the ratio of reflectances, which provides oxygen transmittance, depend on CTOP and CGT variation. This double sensitivity raises the question of the retrieval of CTOP without knowledge about CGT, and that of the simultaneous retrieval of both CTOP and CGT. One way to address these issues could be in the information gained by the angular dependance of the reflectance ratio on CGT and CTOP, as already noted by Ferlay et al. (2010) for optically thick clouds.

For optically thick clouds ($COT = 16$, Fig. 5c), the difference between forward and backward scattering is lowered and is practically null for small geometrical depth as this corresponds to the solid reflector situation already described in Fig. 4c.

For the other case with $COT = 4$ (Fig. 5b), we notice optically thin clouds characteristics for large CGT (differences between back and forward scattering) and thick clouds characteristics for low CGT. As it will be discussed later, this actually reflects the transition from single to multiple scattering regimes as the extinction within the cloud increases.

**Cloud top altitude
and geometrical
thickness study**

G. Merlin et al.

Title Page

Abstract

Introduction

Conclusions

References

Tables

Figures



Back

Close

Full Screen / Esc

Printer-friendly Version

Interactive Discussion



To illustrate the angular A-band ratio dependance on CTOP and CGT, Fig. 6 presents isolines of CTOP and CGT values in a two dimensional space with average band ratio value R , here along the ordinate axis, and the angular standard deviation (σ_R) along the abscissa axis. Values are obtained for the AS 1 (cf. Fig. 2) using same cloud parameters as for Figs. 4 and 5. In practice, we represent here a solution space from which one could attempt to be retrieve CTOP and CGT knowing R and σ_R . Figure 6a–c shows the solution space for, respectively, COT of 1, 4 and 16.

In Fig. 6a (COT = 1), we notice that the curves of constant CTOP (red curves) and CGT (black curves) are well separated. The curves of constant CGT are almost vertical, which means that CTOP is primarily sensitive to R and less dependent on σ_R . Conversely, constant CTOP curves are almost horizontal traducing the fact that CGT is mostly sensitive to σ_R only. Even though the solution space is not orthogonal, this figure shows how R and σ_R could be used to infer both CTOP and CGT. For optically thick clouds (Fig. 6c), the ratio is again sensitive to both parameters but it is important to note that, contrary to small COT, increasing CGT leads here to smaller σ_R . We can relate this observation to the Fig. 5c in which the slope of A-band ratio decreases with CGT, thereby reducing its angular standard deviation. On the contrary, for optically thin clouds and in Fig. 5a, the slope increases when CGT increases (at least for low air mass). This inverse sensitivity of σ_R implies that, between the cases of optically thin and thick clouds, CGT becomes no longer sensitive to the standard deviation. That is confirmed by Fig. 6b (COT = 4) where both parameters are sensitive primarily to R and the solution space collapses along the σ_R axis. This correlation between the sensitivities make it impossible to infer both parameters from the reduced set of R and σ_R metrics. This second qualitative analysis again illustrates how multi-angle A-band ratio measurements above a black surface can potentially convey information on both CTOP and CGT for optically thick, as was already noticed by Ferlay et al. (2010), but also for thin clouds. Between those two cases however, the reduced set of metrics based on A-band differential absorption measurement does not seem to allow simultaneous retrieval of CTOP and CGT.

3.2 Addition of a Lambertian surface

A black surface is a good approximation of the ocean out of the sun glint area. However, for retrievals over land surfaces, we need to extend our model and analysis including more realistic surface reflectance. To focus on the physical understanding of mechanisms contributing to the band ratio signal, we choose to simulate the surface by using a simple Lambertian model with two very different albedo values: 0.2 (corresponding approximately to sand) and 0.8 (fresh snow or ice), thus activating path 3 in Fig. 3.

Figure 7 is the same as Fig. 4 with a surface albedo of 0.2. For COT = 16, the cloud opacity is such that the impact of the surface is negligible. For COT = 1 and 4, differences are notable. The ratios are weaker. Because of surface brightness, the probability of longer pathlength increases, further attenuating radiation in absorbing channels. Indeed, the non-absorbing spectral bands present higher reflectance thanks to the reflection, which can be multiple, between the surface and the cloud. Such reflection for the absorbing band also occurs but the increased absorption limits their contribution to observed TOA reflectance. By adding a bright surface, the out-band radiance increases more than the in-band one, thereby the A-band ratio is reduced. This effect is more important for high cloud top altitudes and low air mass. Indeed, the higher cloud is, the more the photons pathway between the surface and the cloud increases. The difference between in- and out-band is therefore increasing and the band ratio decreases. For COT = 1 and low air mass, it logically appears that the sensitivity to CTOP is extremely low as the cloud does not modify significantly the photon pathway.

Figure 8 is the same as Fig. 5 with a surface albedo of 0.2. Again, a cloud with COT = 16 (Fig. 8c) is very opaque and surface has almost no effect in the oxygen A-band ratio. For COT = 4 and COT = 1, the ratio is also lower. The decrease is higher here for geometrically thick clouds due to the same effect seen through. The multiple reflections between the cloud and the surface increases the photon path, hence the absorption in the in-band. The important parameter to consider is thus the cloud base

Cloud top altitude and geometrical thickness study

G. Merlin et al.

Title Page

Abstract

Introduction

Conclusions

References

Tables

Figures



Back

Close

Full Screen / Esc

Printer-friendly Version

Interactive Discussion



altitude. The higher the cloud base, the more the surface affects the A-band radiance because of the difference between in- and out-band radiances.

Figure 9 is the same than Figs. 4 and 7 and Fig. 10 than Figs. 5 and 8 with a surface albedo of 0.8. With a brighter surface, the effect of the surface is obviously more apparent. For $COT = 1$, the cloud altitude and thickness have almost no impact in the A-band ratio because the radiance coming from the cloud represents a negligible part of the signal. For $COT = 16$, the cloud signal is higher and consequently, the ratio is modified depending on $CTOP$ and CGT .

To summarize, a Lambertian surface decreases A-band sensitivities on both $CTOP$ and CGT for the smallest COT , the COT limit depending on the surface albedo.

4 Theoretical information content study

In order to go further in the sensitivity studies on the O_2 A-band, we performed an information content study based on a Bayesian optimal estimation approach. It also provides an elegant framework to compute the information content of the observing system as well as to perform an error analysis on the resulting retrieval. The formulation of the problem in this study has been developed by Rodgers (1998) and used in previous studies by several authors (Sourdeval et al., 2013, 2014; King and Vaughan, 2012; Cooper et al., 2006).

4.1 Information content theory

Details on how the information content is calculated can be found in the aforementioned studies and, for the sake of completeness, the main theoretical elements are reported in the Appendix. In this section, we simply describe and specify the different parameters used in the Rodgers information content formulation.

For this study, the state vector \mathbf{x} contains the parameters $CTOP$ and CGT and the measurement vector, A-band ratios for the different view angles described in Fig. 2. As

Cloud top altitude and geometrical thickness study

G. Merlin et al.

Title Page

Abstract

Introduction

Conclusions

References

Tables

Figures



Back

Close

Full Screen / Esc

Printer-friendly Version

Interactive Discussion



for non-retrieved parameters, we considered only COT, the effective radius of the cloud particles, and the surface albedo. Preusker and Lindstrot (2009) showed that those parameters are indeed the geophysical quantities that most influence the measured A-band ratio.

The only information we have a priori is that cloud top altitude CTOP cannot be very high and cloud thickness CGT cannot exceed CTOP. Consequently, we considered an a priori standard deviation of 5 km for both CGT and CTOP. The a priori variance–covariance matrix \mathbf{S}_a is assumed diagonal and elements are those variances ($\mathbf{S}_{a,ii} = 5^2, i = 1, 2$). This represents our knowledge of the state vector before the measurements and retrievals are performed. Measurement noise is assumed to be 1 % of the ratio for both MSPI and 3MI. Indeed, the ratio method leads to a smaller noise, which is typically considered to be on of the order of 2–3 % for the radiances themselves. We use this measurement noise estimate to compute a diagonal variance–covariance matrix as

$$\mathbf{S}_{y,ii} = \left(0.01 \times \frac{\text{Rad}_{\text{in},i}}{\text{Rad}_{\text{out},i}} \right)^2$$

for the i th angular measurement, where subscript “out” means either the continuum channel (MSPI or 3MI) or 3MI’s broadband channel.

We introduce also a variance–covariance matrix for the forward model, linked to the non-retrieved parameters. Those parameters are fixed but they are assumed known but only to within a known uncertainty. We considered 10 % relative errors on COT and the effective particle radius, and an absolute error of 0.05 on the surface albedo.

4.2 Inter-comparison of 3MI and MSPI – measurement information content

We use the formalism reminded in the Appendix to study the information content of the three different O_2 A-band measurement configurations described in Sect. 2.3 and perform an inter-comparison for a reference case. The reference case is a homogeneous

Cloud top altitude and geometrical thickness study

G. Merlin et al.

Title Page

Abstract

Introduction

Conclusions

References

Tables

Figures



Back

Close

Full Screen / Esc

Printer-friendly Version

Interactive Discussion



Cloud top altitude and geometrical thickness study

G. Merlin et al.

Title Page

Abstract

Introduction

Conclusions

References

Tables

Figures



Back

Close

Full Screen / Esc

Printer-friendly Version

Interactive Discussion



liquid cloud with an optical thickness of 16, with droplets following a log-normal distribution with an effective radius of 12 μm and an effective variance of 0.02. The surface is assumed black, SZA is fixed at 30°, and we use the angular sampling configuration AS 1 (cf. Fig. 2). We describe and compare the A-band information content provided by the three instrumental configurations by analyzing the partial degrees of freedom and the a posteriori errors (square roots of the diagonal elements of the a posteriori variance–covariance matrix \mathbf{S}_y , as described in the Appendix).

Figure 11 presents an example of the information content of the A-band observations obtained from the three instrumental configurations. In this figure, we have plotted the degrees of freedom (DOFs) and the a posteriori errors in the state space: CGT on the vertical axis for six values ranging from 0.5 to 5 km; CTOP on the horizontal axis for six values ranging from 1 to 6 km. We note that, logically, the higher the information content, the lower the a posteriori errors. We also notice some general similarities between the three configurations. The A-band information on CTOP increases when it increases and CGT decreases. It is the reverse for the information content on CGT that increases with a decrease of CTOP and an increase of CGT. Indeed, when the information on the more sensitive parameter (CTOP) decreases, a part of the lost information is reported to the other parameter (CGT). For the cases with small CGT, there is low information content, showing us that the retrieval of this parameter is not reliable (i.e., $\text{DOF} < 0.5$).

Comparison of Fig. 11a–c (the three rows) shows that information content of 3MI (thin-band/broad-band) is lower than 3MI (in-band/out-band) that is in turn lower than MSPI. The in/out-band configuration is thus more effective than the thin/broad band one. Even if MSPI has less view angles than 3MI, it provides higher information. We can therefore conclude that MSPI's spectral channel definitions are more suitable than those of 3MI for the current application.

The DOF (per retrieved parameter) and a posteriori error are obviously linked. In the following, we will therefore only consider the DOFs. Moreover, respective performances and differences between those spectral configuration are fairly invariant for the cases studied. For analysis of multi-angle observation, we therefore only present and discuss

Cloud top altitude and geometrical thickness study

G. Merlin et al.

Title Page

Abstract

Introduction

Conclusions

References

Tables

Figures



Back

Close

Full Screen / Esc

Printer-friendly Version

Interactive Discussion



edge be available on CTOP. We also notice that some limited additional information is likewise brought on CTOP for low CGT and high CTOP. It means that A-band ratio is able to reduce the a priori volume even if this one is already small. Again, and as already discussed by Preusker and Lindstrot (2009), these results simply illustrate that mono-angular A-band measurement can be used to retrieve CTOP without knowledge of CGT. When a priori knowledge on CTOP is provided, CGT could potentially be retrieved from single view observation.

This conclusion should however be considered in view of our present assumption that other non-retrieved parameters, such as COT or particle size, are quite well known. We then anticipate that multi-angle measurements will be more robust to noise but it remains to be investigated how the various errors on measurements and non-retrieved parameters impact the a posteriori errors on CGT for single-view or multi-angular observations. This issue is clearly out-of-scope for our present study since we focus on multi-angle measurements to retrieve simultaneously CTOP and CGT with no further a priori information on either (beyond that encapsulated in \mathbf{S}_a).

4.3 Cloud optical thickness variation

The effect of the optical thickness on measurement sensibilities were examined previously. Here, we study it in term of information content in order to take into account the measurement noise and uncertainty in non-retrieved parameters (COT and effective radius, the surface being considered black in this case).

Figure 13 shows information content of 3MI A-band ratio for the reference case as well as for several other optical thicknesses (same ones as in Sect. 3). The information content is, for optically thick (COT = 16) or thin (COT = 1) clouds, pretty close and significantly higher than for the intermediate optical thickness (COT = 4). This confirms the finding in Fig. 6, where the LUT representation shows that retrieval of both CGT and CTOP is not feasible. The joint retrieval should however be possible for optically thin and thick clouds; the problem being to determine the limit between those cases as it could depend on cloud microphysics and/or on illumination and viewing geometry.

Cloud top altitude and geometrical thickness study

G. Merlin et al.

Title Page

Abstract

Introduction

Conclusions

References

Tables

Figures



Back

Close

Full Screen / Esc

Printer-friendly Version

Interactive Discussion



did not always *-count for measurement noise and errors due to uncertainties in the non-retrieved parameters, and were limited to thick clouds above black surfaces. In this study, we consider optically thick clouds as well as optically intermediate and thin clouds. In addition, we look at the information content above Lambertian surfaces with moderate and high albedo. Main results are:

1. MSPI's configuration seems to be more appropriate and the use of an external non-absorbing band seems more efficient than a broad spectral channel covering the A-band and some neighboring continuum wavelengths.
2. Information on CTOP is high in almost all studied cases and this parameter seems to be retrievable using an optimal estimation scheme.
3. The retrieval of CGT seems to pose problems in some cases. Over a black surface, information could be too low for CGT smaller than 1–2 km. Over a brighter surface, this information is decreased for most of cases, but not for optically thick clouds.

Interestingly, sensitivity to CGT increases for relatively thick ($CGT \gtrsim \max\{2, CTOP - 2\}$ km) clouds of intermediate optical thickness ($COT \approx 4$) when they occur over the brightest surfaces, due to the extra pathlength cumulated in the cloud after surface reflection.

This study aimed to determine the capabilities of multi-angle A-band measurements, but other spectral regions could be useful to retrieve CTOP and CGT. For instance, polarized radiances in the deep blue are sensitive to CTOP (Goloub et al., 1994). It shall be noted that other planned or already launched missions carrying sensors that provide measurements in the O_2 A- and B-bands could still benefit from our analysis. We can take as examples the Japanese Second generation Global Imager of the Global Change Observation Mission – Climate (SGLI/GCOM-C) and the Earth Polychromatic Imaging Camera on the DSCOVR spacecraft (EPIC/DSCOVR) that observes the sunlit Earth from the Lagrange “L1” point. Additionally, but out-of-scope of the present

study, A-band measurements at high spectral resolution from OCO-2 or GOSAT, even at a single view angle, could also be used to retrieve similar cloud information with the additional limitation of coarse spatial resolution leading to larger uncertainties in the forward model.

5 Appendix A: The optimal estimation approach to information content analysis

In the Rodgers (2000) formalism for the optimal estimation of model parameters from observations, measurements are represented by the “data” m vector \mathbf{y} (in this study containing the multi-angle suite of A-band ratios, e.g., $m = 9$ and 15 respectively for MSPI and 3MI) and the retrieved parameters are contained in the “state” n vector \mathbf{x} (here containing CTOP and CGT, i.e., $n = 2$). The corresponding information content theory uses Gaussian probability functions (PDFs) to relate, through Bayes’ theorem, the measurement space and the state space. Since the PDFs are assumed to follow multi-variate Gaussian distributions, they are defined by their means and variance–covariance matrices:

- 15 – \mathbf{S}_a for the PDF of the a priori state vector representing our “knowledge” of the state vector before any measurements are made;
- \mathbf{S}_x for the PDF of the a posteriori state vector representing our “knowledge” of the state vector accounting for the measurements;
- \mathbf{S}_e represents the variance–covariance matrix of the measurement and the forward model errors.

We first need to define the forward model variance–covariance matrix and particularly errors due to the non-retrieved parameters we use in the forward model. \mathbf{S}_b will be the variance–covariance matrix of those non-retrieved parameters (assumed diagonal). The variance–covariance matrix associated to the model errors \mathbf{S}_f is therefore

Cloud top altitude and geometrical thickness study

G. Merlin et al.

Title Page

Abstract

Introduction

Conclusions

References

Tables

Figures



Back

Close

Full Screen / Esc

Printer-friendly Version

Interactive Discussion



computed as

$$\mathbf{S}_f = \mathbf{K}_b \mathbf{S}_b \mathbf{K}_b^T, \quad (\text{A1})$$

with \mathbf{K}_b being the Jacobian of the non-retrieved parameters, which represents the sensitivity of the forward model to those non-retrieved parameters, and superscript “T” meaning transpose.

We can then compute the variance–covariance matrix \mathbf{S}_e of the measurements and forward model errors, respectively \mathbf{S}_y , \mathbf{S}_f :

$$\mathbf{S}_e = \mathbf{S}_y + \mathbf{S}_f. \quad (\text{A2})$$

The a posteriori variance–covariance matrix \mathbf{S}_x , with the diagonal elements representing the uncertainties on the best retrieval, is expressed as

$$\mathbf{S}_x = \left(\mathbf{S}_a^{-1} + \mathbf{K}^T \mathbf{S}_e^{-1} \mathbf{K} \right)^{-1}. \quad (\text{A3})$$

The term \mathbf{K} represents the kernel (or Jacobian) matrix, which describes the sensitivity of the forward model to each parameter to be retrieved. A posteriori retrieval errors for the i th parameter is

$$\sigma_i = \sqrt{\mathbf{S}_{x,ii}}. \quad (\text{A4})$$

The notion of information content was introduced by Shannon (1948). They developed this theory by establishing an analogy between the information carried by a signal and the entropy of its PDF. Later, Rodgers (2000) applied this idea to his formalism. He defined the information content H_s of measurements by the difference between the a priori and a posteriori entropies of the respective gaussian PDFs defined by the matrices \mathbf{S}_a and \mathbf{S}_x :

$$H_s = \frac{1}{2} \log_2 \left(\|\mathbf{S}_x \mathbf{S}_a^{-1}\| \right). \quad (\text{A5})$$

Cloud top altitude and geometrical thickness study

G. Merlin et al.

Title Page

Abstract

Introduction

Conclusions

References

Tables

Figures

⏪

⏩

◀

▶

Back

Close

Full Screen / Esc

Printer-friendly Version

Interactive Discussion



H_s thus quantifies the reduction of the number of possible states from the a priori state space to the best-estimate a posteriori state space. Rodgers describes another way of quantifying this volume reduction, by using the “averaging kernel” matrix:

$$A = \frac{\partial \hat{\mathbf{x}}}{\partial \mathbf{x}}, \quad (\text{A6})$$

5 with $\hat{\mathbf{x}}$ representing the best estimate of the state vector and \mathbf{x} the true state vector. A is therefore the sensitivity of the retrieval to the true state. It is a simple function of the a priori and a posteriori volumes:

$$A = I_n - \mathbf{S}_x \mathbf{S}_a^{-1}, \quad (\text{A7})$$

10 where I_n is the $n \times n$ identity matrix. From Eqs. (A5) and (A7), we can express the information content H_s as:

$$H_s = \frac{1}{2} \log_2 (\|I_n - A\|). \quad (\text{A8})$$

15 We can also express the total number of degrees of freedom d_s as a function of the averaging kernel matrix. The degree of freedom is a measure of the number of independent pieces of information contained in the observing system. It is expressed as

$$d_s = \text{Tr}(A). \quad (\text{A9})$$

Note that its maximum value is equal to the dimension n of the state vector. We can also get the *partial* degree of freedom of the i th parameter attached to each element of the state vector of \mathbf{x} :

$$20 \quad d_{s,i} = A_{ii}. \quad (\text{A10})$$

It represents the information brought by the measurements on the parameter x_i ($i = 1, \dots, n$).

Cloud top altitude and geometrical thickness study

G. Merlin et al.

Title Page	
Abstract	Introduction
Conclusions	References
Tables	Figures
◀	▶
◀	▶
Back	Close
Full Screen / Esc	
Printer-friendly Version	
Interactive Discussion	



Cloud top altitude and geometrical thickness study

G. Merlin et al.

Title Page

Abstract

Introduction

Conclusions

References

Tables

Figures



Back

Close

Full Screen / Esc

Printer-friendly Version

Interactive Discussion



This partial degree of freedom is a very practical tool for quantifying information content. Indeed, $d_{s,i}$ lies between 0 and 1, with a low value representing a low information and conversely when it approaches unity. Partial degree of freedom is therefore what we use throughout our study, with the a posteriori variance–covariance matrix \mathbf{S}_x in Eq. (A3), to study the information content of our measurements, namely, multi-angle O_2 A-band “in/out” ratios. Note that, from Eq. (A4) on the one hand, from Eqs. (A7) and (A10) on the other hand, that $d_{s,i}$ increases when σ_i decreases.

Acknowledgements. The authors are grateful for financial support from CNES as well as NASA’s SMD/ESD (several programs managed by H. Maring, K. Jucks, and R. Eckman). They also thank Dave Diner, Jay Herman, and Yuequi Yang for fruitful discussions. Guillaume Merlin is supported by a PhD grad from CNES and Région Nord-Pas de Calais.

References

- Bréon, F.-M. and Doutriaux-Boucher, M.: A comparison of cloud droplet radii measured from space, *IEEE T. Geosci. Remote*, 43, 1796–1805, doi:10.1109/TGRS.2005.852838, 2005. 12713
- Cooper, S. J., L’Ecuyer, T. S., Gabriel, P., Baran, A. J., and Stephens, G. L.: Objective assessment of the information content of visible and infrared radiance measurements for cloud microphysical property retrievals over the global oceans. Part II: Ice clouds, *J. Appl. Meteorol. Clim.*, 45, 42–62, doi:10.1175/JAM2327.1, 2006. 12723
- Davis, A., Polonsky, I., and Marshak, A.: Space-time Green functions for diffusive radiation transport, in application to active and passive cloud probing, in: *Light Scattering Reviews*, vol. 4, edited by: Kokhanovsky, A., Springer-Praxis, Heidelberg (Germany), 169–292, 2009. 12712, 12719, 12728
- de Beek, R., Vountas, M., Rozanov, V. V., Richter, A., and Burrows, J. P.: The ring effect in the cloudy atmosphere, *Geophys. Res. Lett.*, 28, 721–724, doi:10.1029/2000GL012240, 2001. 12711
- de Haan, J., Bosma, P., and Hovenier, J.: The adding method for multiple scattering calculations of polarized light, *Astron. Astrophys.*, 183, 371–391, 1987. 12717

Cloud top altitude and geometrical thickness study

G. Merlin et al.

Title Page

Abstract

Introduction

Conclusions

References

Tables

Figures



Back

Close

Full Screen / Esc

Printer-friendly Version

Interactive Discussion



Desmons, M., Ferlay, N., Parol, F., Mcharek, L., and Vanbauce, C.: Improved information about the vertical location and extent of monolayer clouds from POLDER3 measurements in the oxygen A-band, *Atmos. Meas. Tech.*, 6, 2221–2238, doi:10.5194/amt-6-2221-2013, 2013. 12711, 12712, 12713, 12718

5 Diner, D. J., Davis, A., Hancock, B., Geier, S., Rheingans, B., Jovanovic, V., Bull, M., Rider, D. M., Chipman, R. A., Mahler, A.-B., and McClain, S. C.: First results from a dual photoelastic-modulator-based polarimetric camera, *Appl. Optics*, 49, 2929–2946, 2010. 12715

10 Diner, D. J., Xu, F., Garay, M. J., Martonchik, J. V., Rheingans, B. E., Geier, S., Davis, A., Hancock, B. R., Jovanovic, V. M., Bull, M. A., Capraro, K., Chipman, R. A., and McClain, S. C.: The Airborne Multiangle SpectroPolarimetric Imager (AirMSPI): a new tool for aerosol and cloud remote sensing, *Atmos. Meas. Tech.*, 6, 2007–2025, doi:10.5194/amt-6-2007-2013, 2013. 12715

15 Ferlay, N., Thieuleux, F., Cornet, C., Davis, A. B., Dubuisson, P., Ducos, F., Parol, F., Riédi, J., and Vanbauce, C.: Toward new inferences about cloud structures from multidirectional measurements in the oxygen A band: middle-of-cloud pressure and cloud geometrical thickness from POLDER-3/PARASOL, *J. Appl. Meteorol. Clim.*, 49, 2492–2507, doi:10.1175/2010JAMC2550.1, 2010. 12711, 12712, 12713, 12718, 12719, 12720, 12721

20 Goloub, P., Deuze, J. L., Herman, M., and Fouquart, Y.: Analysis of the POLDER polarization measurements performed over cloud covers, *IEEE T. Geosci. Remote*, 32, 78–88, doi:10.1109/36.285191, 1994. 12711, 12731

Joiner, J. and Bhartia, P. K.: The determination of cloud pressures from rotational Raman scattering in satellite backscatter ultraviolet measurements, *J. Geophys. Res.*, 100, 23019–23026, doi:10.1029/95JD02675, 1995. 12711

25 King, M. D., Kaufman, Y. J., Menzel, W. P., and Tanre, D.: Remote sensing of cloud, aerosol, and water vapor properties from the Moderate Resolution Imaging Spectrometer (MODIS), *IEEE T. Geosci. Remote*, 30, 2–27, 1992. 12711

30 King, N. J. and Vaughan, G.: Using passive remote sensing to retrieve the vertical variation of cloud droplet size in marine stratocumulus: an assessment of information content and the potential for improved retrievals from hyperspectral measurements, *J. Geophys. Res.*, 117, D15206, doi:10.1029/2012JD017896, 2012. 12723

**Cloud top altitude
and geometrical
thickness study**

G. Merlin et al.

Title Page

Abstract

Introduction

Conclusions

References

Tables

Figures



Back

Close

Full Screen / Esc

Printer-friendly Version

Interactive Discussion



- Knibbe, W. J. J., De Haan, J. F., Hovenier, J. W., Stam, D. M., Koelemeijer, R. B. A., and Stammes, P.: Deriving terrestrial cloud top pressure from photopolarimetry of reflected light, *J. Quant. Spectrosc. Ra.*, 64, 173–199, doi:10.1016/S0022-4073(98)00135-6, 2000. 12711
- Kratz, D. P.: The correlated k distribution technique as applied to the AVHRR channels, *J. Quant. Spectrosc. Ra.*, 53, 501–517, doi:10.1016/0022-4073(95)90050-0, 1995. 12717
- Mace, G. G., Zhang, Q., Vaughan, M., Marchand, R., Stephens, G., Trepte, C., and Winker, D.: A description of hydrometeor layer occurrence statistics derived from the first year of merged Cloudsat and CALIPSO data, *J. Geophys. Res.*, 114, D00A26, doi:10.1029/2007JD009755, 2009. 12711
- Moroney, C., Davies, R., and Muller, J.-P.: Operational retrieval of cloud-top heights using MISR data, *IEEE T. Geosci. Remote*, 40, 1532–1540, doi:10.1109/TGRS.2002.801150, 2002. 12712
- Platnick, S., King, M. D., Ackerman, S., Menzel, W. P., Baum, B., Riedi, J. C., and Frey, R.: The MODIS cloud products: algorithms and examples from Terra, *IEEE T. Geosci. Remote*, 41, 459–473, doi:10.1109/TGRS.2002.808301, 2003. 12711, 12726
- Preusker, R. and Lindstrot, R.: Remote sensing of cloud-top pressure using moderately resolved measurements within the oxygen A band – a sensitivity study, *J. Appl. Meteorol. Clim.*, 48, 1562–1574, doi:10.1175/2009JAMC2074.1, 2009. 12712, 12724, 12726, 12727
- Ramon, D., Richard, S., and Dubuisson, P.: MERIS in-flight spectral calibration in O₂ absorption using surface pressure retrieval, *Proc. SPIE*, 4891, 505–514, 2003. 12714, 12716
- Riedi, J., Marchant, B., Platnick, S., Baum, B. A., Thieuleux, F., Oudard, C., Parol, F., Nicolas, J.-M., and Dubuisson, P.: Cloud thermodynamic phase inferred from merged POLDER and MODIS data, *Atmos. Chem. Phys.*, 10, 11851–11865, doi:10.5194/acp-10-11851-2010, 2010. 12713
- Rodgers, C. D.: Information Content and Optimisation of High Spectral Resolution Remote Measurements, 21, 361–367, doi:10.1016/S0273-1177(97)00915-0, 1998. 12723
- Rodgers, C. D.: *Inverse Methods for Atmospheric Sounding: Theory and Practice*, World Scientific, Singapore, 2000. 12732, 12733
- Rossow, W. B. and Schiffer, R. A.: ISCCP cloud data products, *B. Am. Meteor. Soc.*, 72, 2–20, doi:10.1175/1520-0477(1991)072<0002:ICDP>2.0.CO;2, 1991. 12711
- Rozañov, V. V. and Kokhanovsky, A. A.: Semianalytical cloud retrieval algorithm as applied to the cloud top altitude and the cloud geometrical thickness determination from top-of-

Cloud top altitude and geometrical thickness study

G. Merlin et al.

Title Page

Abstract

Introduction

Conclusions

References

Tables

Figures



Back

Close

Full Screen / Esc

Printer-friendly Version

Interactive Discussion



- atmosphere reflectance measurements in the oxygen A band, *J. Geophys. Res.-Atmos.*, 109, D05202, doi:10.1029/2003JD004104, 2004. 12712, 12719
- Schuessler, O., Rodriguez, D. G. L., Doicu, A., and Spurr, R.: Information content in the oxygen-band for the retrieval of macrophysical cloud parameters, *IEEE T. Geosci. Remote*, 52, 3246–3255, 2014. 12712, 12718
- 5 Seiz, G., Tjemkes, S., and Watts, P.: Multiview cloud-top height and wind retrieval with photogrammetric methods: application to Meteosat-8 HRV observations, *J. Appl. Meteorol. Clim.*, 46, 1182–1195, doi:10.1175/JAM2532.1, 2007. 12712
- Shannon, C. E.: A mathematical theory of communication, *Bell Syst. Tech. J.*, 27, 379–423, 1948. 12733
- 10 Sourdeval, O., C-Labonnote, L., Brogniez, G., Jourdan, O., Pelon, J., and Garnier, A.: A variational approach for retrieving ice cloud properties from infrared measurements: application in the context of two IIR validation campaigns, *Atmos. Chem. Phys.*, 13, 8229–8244, doi:10.5194/acp-13-8229-2013, 2013. 12723
- 15 Sourdeval, O., C-Labonnote, L., Baran, A. J., and Brogniez, G.: A methodology for simultaneous retrieval of ice and liquid water cloud properties. Part I: Information content and case study, *Q. J. Roy. Meteor. Soc.*, 141, 870–882, doi:10.1002/qj.2405, 2014. 12723
- Stocker, T., Qin, D., Plattner, G.-K., Tignor, M., Allen, S., Boschung, J., Nauels, A., Xia, Y., Bex, V., and Midgley, P.: IPCC 2013: Climate Change 2013: the Physical Science Basis, contribution of Working Group I to the Fifth Assessment Report of the Intergovernmental Panel on Climate Change, Tech. rep., Cambridge University Press, Cambridge, United Kingdom and New York, NY, USA, 2013. 12711
- 20 Winker, D. M. and Trepte, C. R.: Laminar cirrus observed near the tropical tropopause by LITE, *Geophys. Res. Lett.*, 25, 3351–3354, doi:10.1029/98GL01292, 1998. 12711
- 25 Winker, D. M., Hunt, W. H., and McGill, M. J.: Initial performance assessment of CALIOP, *Geophys. Res. Lett.*, 34, L19803, doi:10.1029/2007GL030135, 2007. 12711
- Wu, D. L., Ackerman, S. A., Davies, R., Diner, D. J., Garay, M. J., Kahn, B. H., Maddux, B. C., Moroney, C. M., Stephens, G. L., Veeffkind, J. P., and Vaughan, M. A.: Vertical distributions and relationships of cloud occurrence frequency as observed by MISR, AIRS, MODIS, OMI, CALIPSO, and CloudSat, *Geophys. Res. Lett.*, 36, L09821, doi:10.1029/2009GL037464, 2009. 12712
- 30 Yamamoto, G. and Wark, D. Q.: Discussion of the letter by R. A. Hanel, “Determination of cloud altitude from a satellite”, 66, 3596–3596, doi:10.1029/JZ066i010p03596, 1961. 12712

Cloud top altitude and geometrical thickness study

G. Merlin et al.

Title Page

Abstract

Introduction

Conclusions

References

Tables

Figures



Back

Close

Full Screen / Esc

Printer-friendly Version

Interactive Discussion



- Yang, Y., Marshak, A., Mao, J., Lyapustin, A., and Herman, J.: A method of retrieving cloud top height and cloud geometrical thickness with oxygen A and B bands for the Deep Space Climate Observatory (DSCOVR) mission: radiative transfer simulations, *J. Quant. Spectrosc. Ra.*, 122, 141–149, doi:10.1016/j.jqsrt.2012.09.017, 2013. 12712, 12718, 12719
- 5 Zhang, Z., Yang, P., Kattawar, G., Riedi, J., C-Labonnote, L., Baum, B. A., Platnick, S., and Huang, H.-L.: Influence of ice particle model on satellite ice cloud retrieval: lessons learned from MODIS and POLDER cloud product comparison, *Atmos. Chem. Phys.*, 9, 7115–7129, doi:10.5194/acp-9-7115-2009, 2009. 12713

Cloud top altitude and geometrical thickness study

G. Merlin et al.

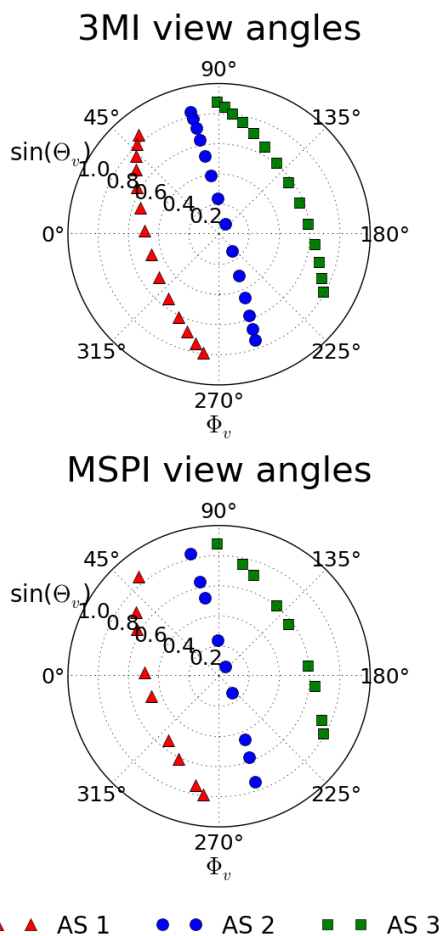


Figure 2. Angular sampling from the choice of MSPI's and 3MI's view angles.

Title Page	
Abstract	Introduction
Conclusions	References
Tables	Figures
◀	▶
◀	▶
Back	Close
Full Screen / Esc	
Printer-friendly Version	
Interactive Discussion	



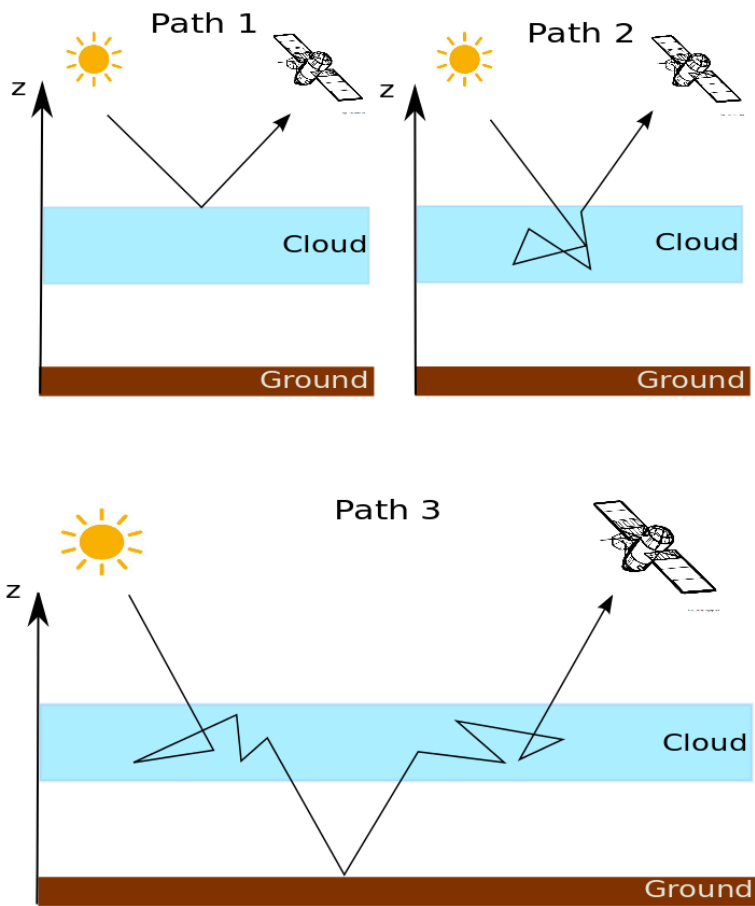


Figure 3. Basic pathways for a reflected photon by the atmosphere–surface system to reach the sensors. Molecular reflection which is weak is not prented.

Cloud top altitude and geometrical thickness study

G. Merlin et al.

Title Page	
Abstract	Introduction
Conclusions	References
Tables	Figures
◀	▶
◀	▶
Back	Close
Full Screen / Esc	
Printer-friendly Version	
Interactive Discussion	



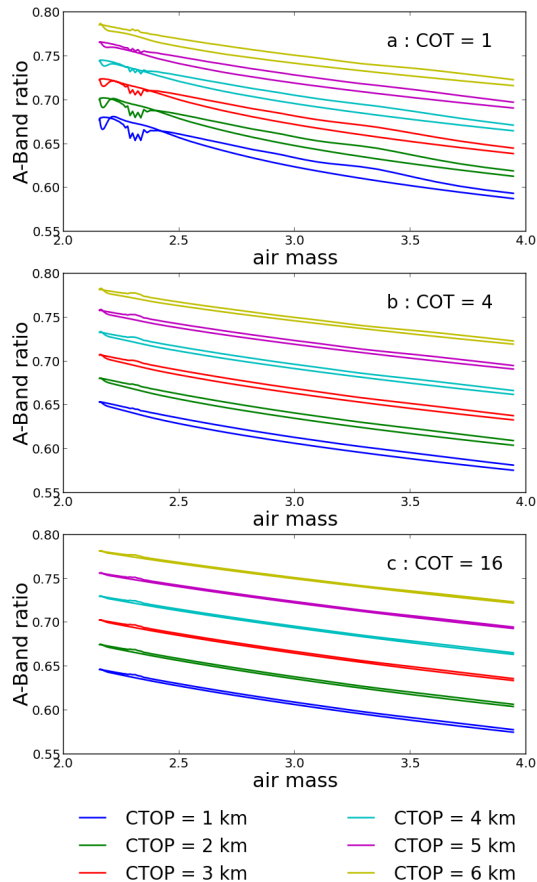


Figure 4. Effect of cloud top altitude variation CTOP on the band ratio. CGT = 0.5 km, SZA = 30°, VAA = 0°, **(a)** COT = 1, **(b)** COT = 4, **(c)** COT = 16.

Cloud top altitude and geometrical thickness study

G. Merlin et al.

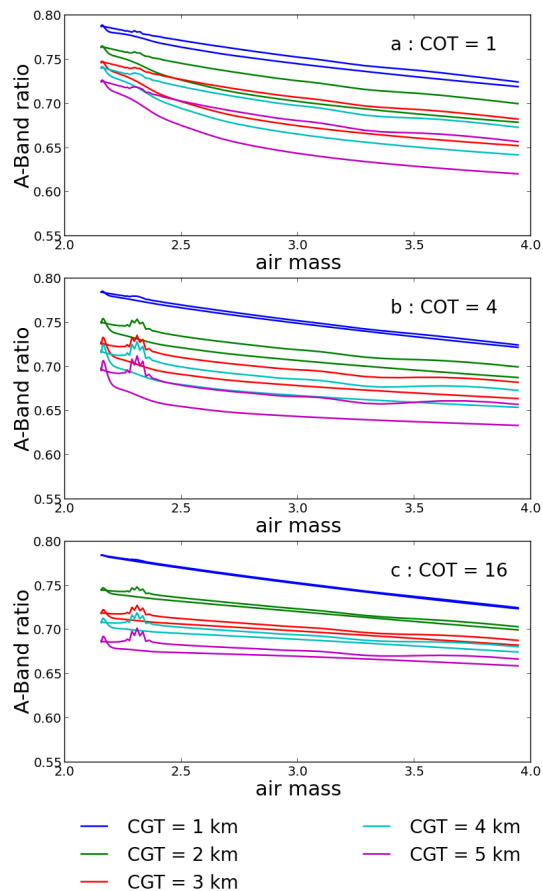


Figure 5. Effect of cloud geometrical thickness variation CGT on the band ratio. $\text{SZA} = 30^\circ$, $\text{VAA} = 0^\circ$, $\text{CTOP} = 6 \text{ km}$, **(a)** $\text{COT} = 1$, **(b)** $\text{COT} = 4$, **(c)** $\text{COT} = 16$.

[Title Page](#)
[Abstract](#)
[Introduction](#)
[Conclusions](#)
[References](#)
[Tables](#)
[Figures](#)
[◀](#)
[▶](#)
[◀](#)
[▶](#)
[Back](#)
[Close](#)
[Full Screen / Esc](#)
[Printer-friendly Version](#)
[Interactive Discussion](#)


Cloud top altitude and geometrical thickness study

G. Merlin et al.

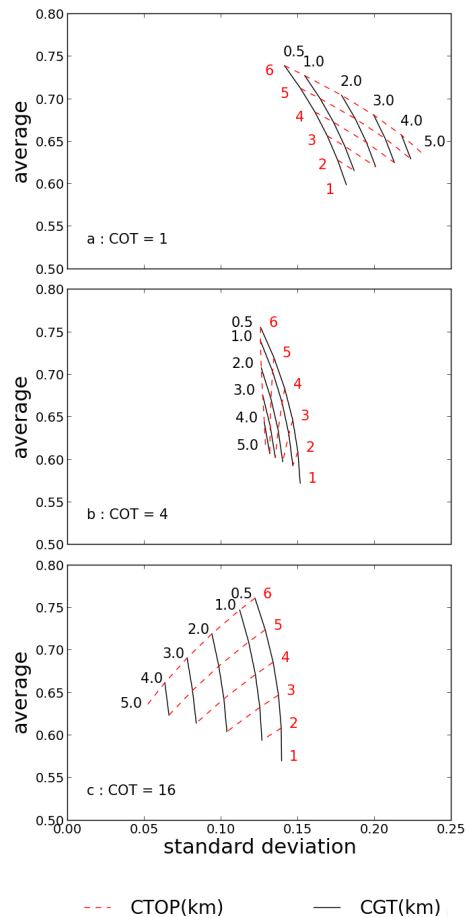


Figure 6. Look up tables for different cloud top height CTOP and cloud optical thickness CGT simultaneously of average and angular standard deviation of the 3MI's A-band ratio. In red, CTOP values and in black, CGT values: **(a)** COT = 1, **(b)** COT = 4, **(c)** COT = 16.

Title Page

Abstract

Introduction

Conclusions

References

Tables

Figures



Back

Close

Full Screen / Esc

Printer-friendly Version

Interactive Discussion



Cloud top altitude and geometrical thickness study

G. Merlin et al.

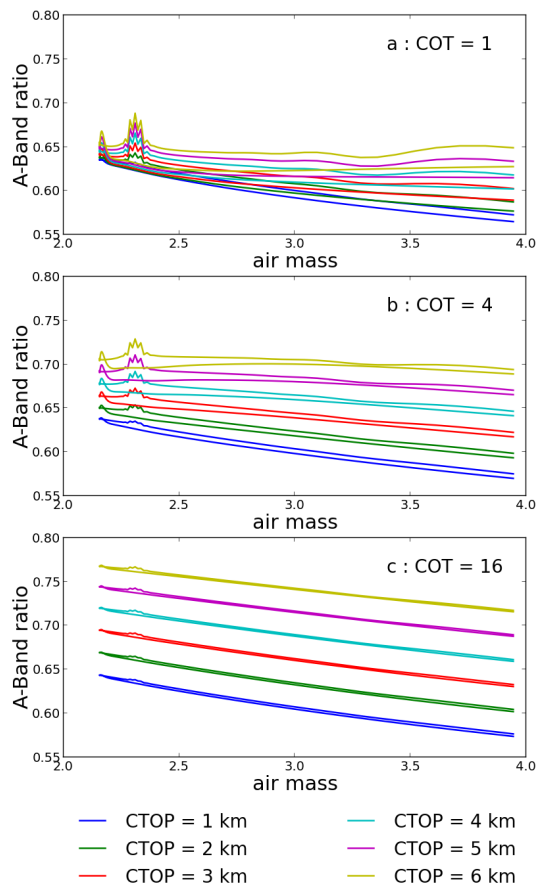


Figure 7. Same as Fig. 4 with a surface albedo of 0.2. **(a)** COT = 1, **(b)** COT = 4, **(c)** COT = 16.

Cloud top altitude
and geometrical
thickness study

G. Merlin et al.

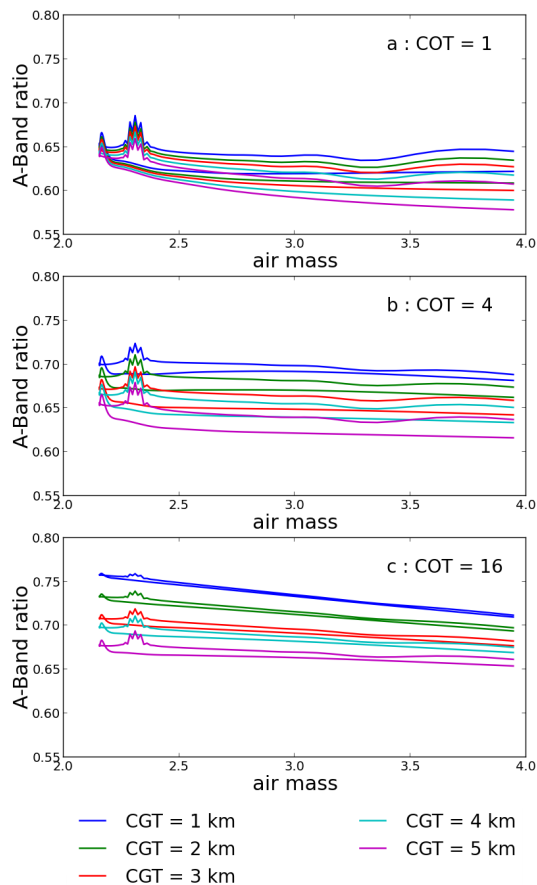


Figure 8. Same as Fig. 5 with a surface albedo of 0.2. **(a)** COT = 1, **(b)** COT = 4, **(c)** COT = 16.

Cloud top altitude and geometrical thickness study

G. Merlin et al.

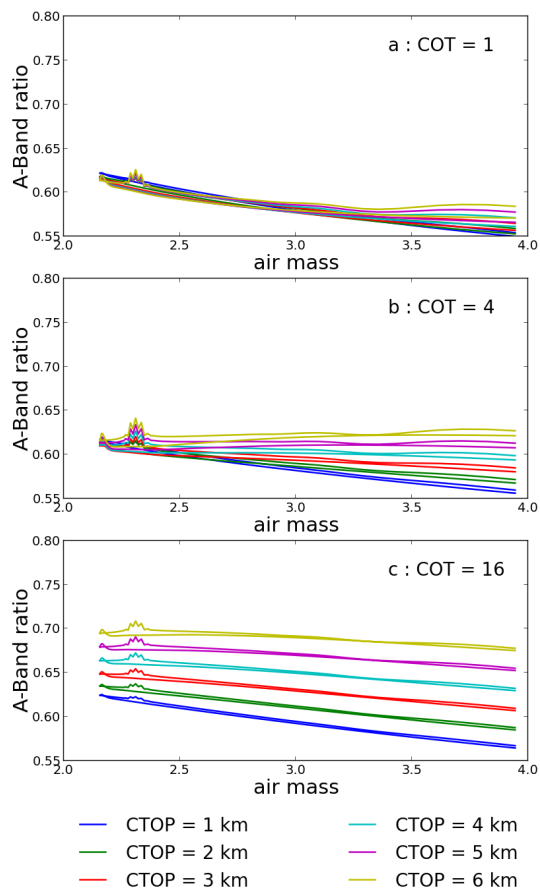


Figure 9. Same as Figs. 4 and 7 with a surface albedo of 0.8. **(a)** COT = 1, **(b)** COT = 4, **(c)** COT = 16.

Cloud top altitude
and geometrical
thickness study

G. Merlin et al.

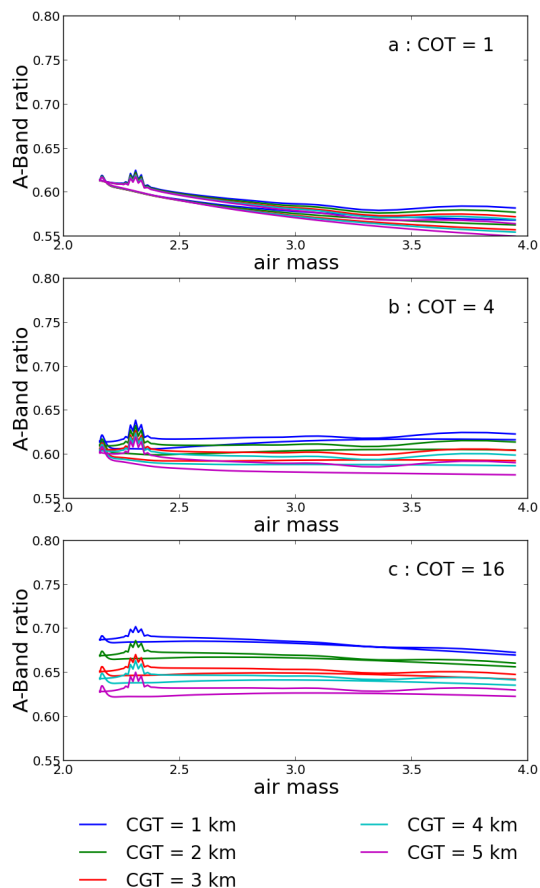


Figure 10. Same as Figs. 5 and 8 with a surface albedo of 0.8. **(a)** COT = 1, **(b)** COT = 4, **(c)** COT = 16.

Cloud top altitude and geometrical thickness study

G. Merlin et al.

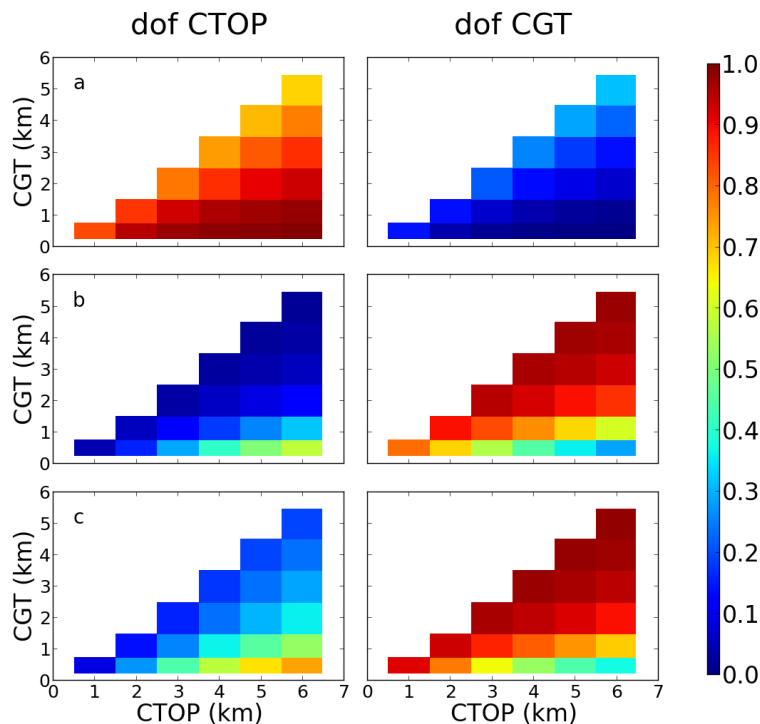


Figure 12. Comparison between mono- and multi-angular A-Band ratio with MSPI's configuration: **(a)** mono-angular A-band ratio DOF ($VZA = 0^\circ$, nadir), **(b)** same as **(a)** with a reduced a priori standard deviation on CTOP (0.5 km), and **(c)** same as **(b)** for multi-angular measurements (orbit/AS 1). $COT = 16$, $r_{\text{eff}} = 12 \mu\text{m}$, $v_{\text{eff}} = 0.02$, $SZA = 30^\circ$.

Title Page

Abstract

Introduction

Conclusions

References

Tables

Figures

◀

▶

◀

▶

Back

Close

Full Screen / Esc

Printer-friendly Version

Interactive Discussion



Cloud top altitude and geometrical thickness study

G. Merlin et al.

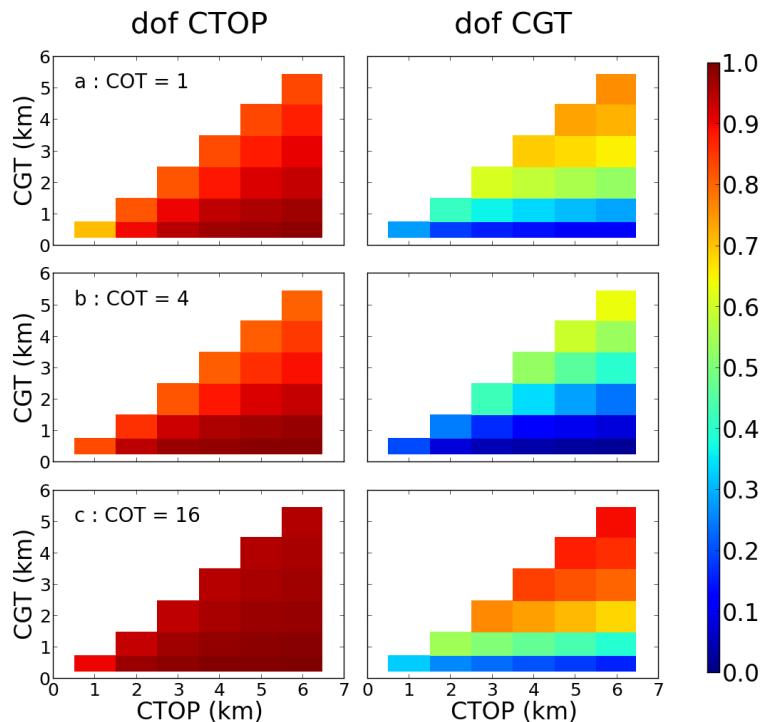


Figure 13. Information content of 3MI A-band for different COTs: **(a)** COT = 1, **(b)** COT = 4, **(c)** COT = 16. Partial DOFs for CTOP (left) and CGT (right).

Cloud top altitude and geometrical thickness study

G. Merlin et al.

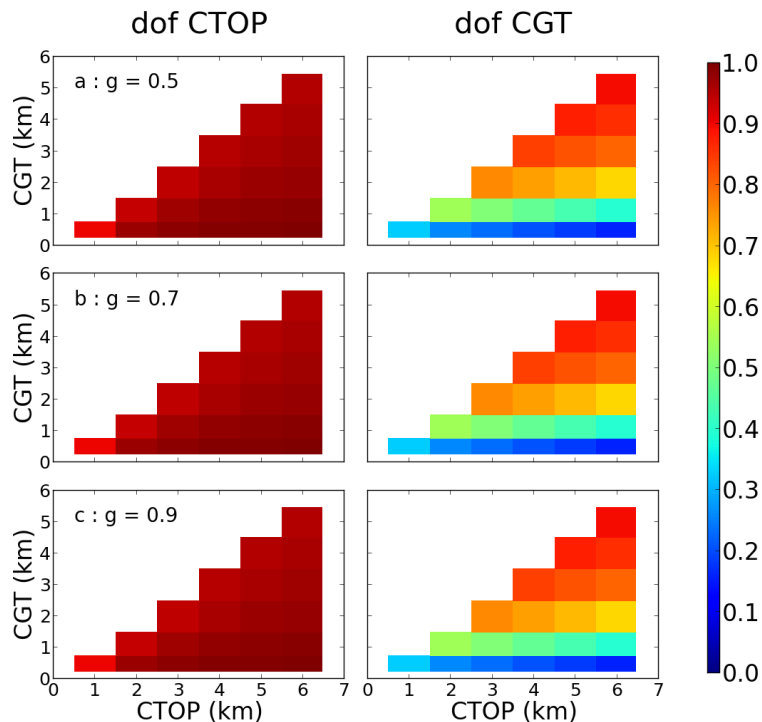


Figure 14. Information content of 3MI A-band with a COT of 16 for different asymmetry factors: (a) $g = 0.5$, (b) $g = 0.7$, (c) $g = 0.9$. Partial DOFs for CTOP (left) and CGT (right).

Title Page

Abstract

Introduction

Conclusions

References

Tables

Figures

◀

▶

◀

▶

Back

Close

Full Screen / Esc

Printer-friendly Version

Interactive Discussion



Cloud top altitude and geometrical thickness study

G. Merlin et al.

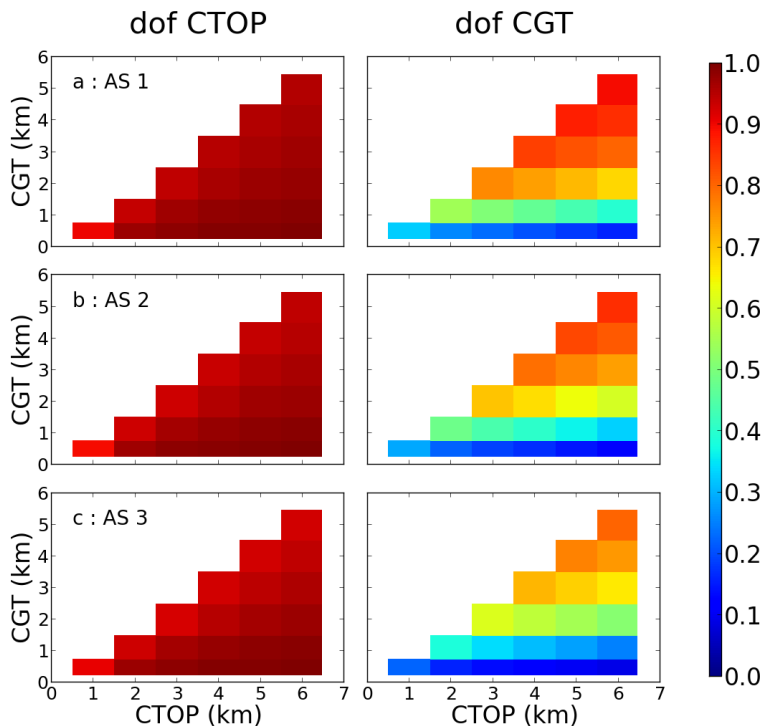


Figure 15. Information content of 3MI A-band with a COT of 16 for different orbits, hence angular samplings: **(a)** AS 1, **(b)** AS 2, **(c)** AS 3. Partial DOFs for CTOP (left) and CGT (right).

Title Page

Abstract

Introduction

Conclusions

References

Tables

Figures

◀

▶

◀

▶

Back

Close

Full Screen / Esc

Printer-friendly Version

Interactive Discussion



Cloud top altitude and geometrical thickness study

G. Merlin et al.

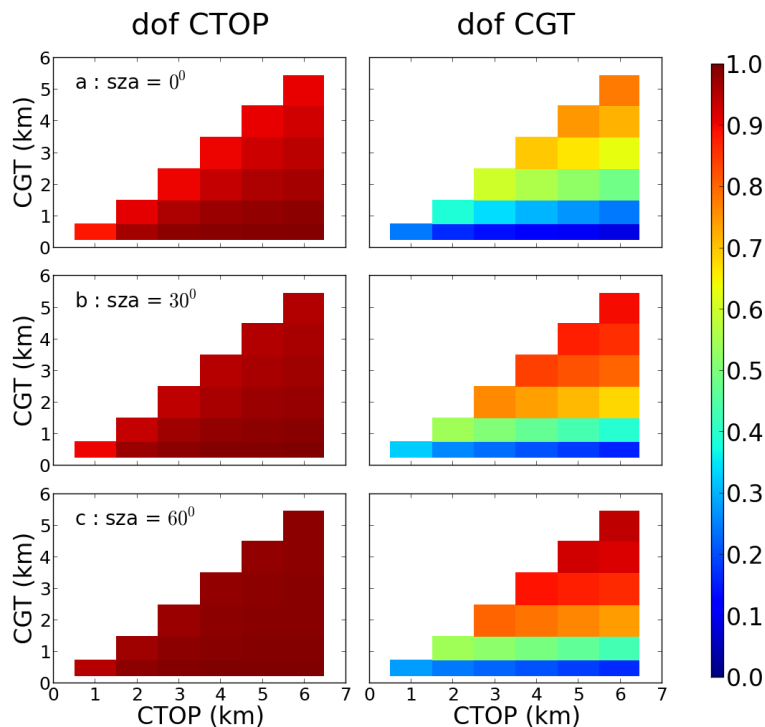


Figure 16. Information content of 3MI A-band with a COT of 16 for different illumination angles: **(a)** SZA = 0° , **(b)** SZA = 30° , **(c)** SZA = 60° . Partial DOFs for CTOP (left) and CGT (right).

Title Page

Abstract

Introduction

Conclusions

References

Tables

Figures

◀

▶

◀

▶

Back

Close

Full Screen / Esc

Printer-friendly Version

Interactive Discussion



Cloud top altitude and geometrical thickness study

G. Merlin et al.

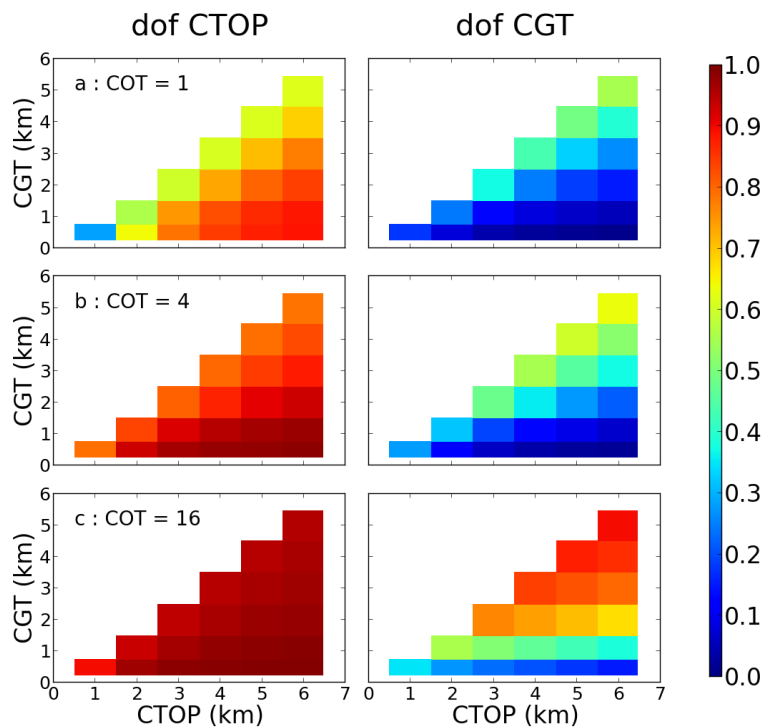


Figure 17. Same as Fig. 13 with an albedo of 0.2.

Title Page

Abstract Introduction

Conclusions References

Tables Figures

◀ ▶

◀ ▶

Back Close

Full Screen / Esc

Printer-friendly Version

Interactive Discussion



Cloud top altitude and geometrical thickness study

G. Merlin et al.

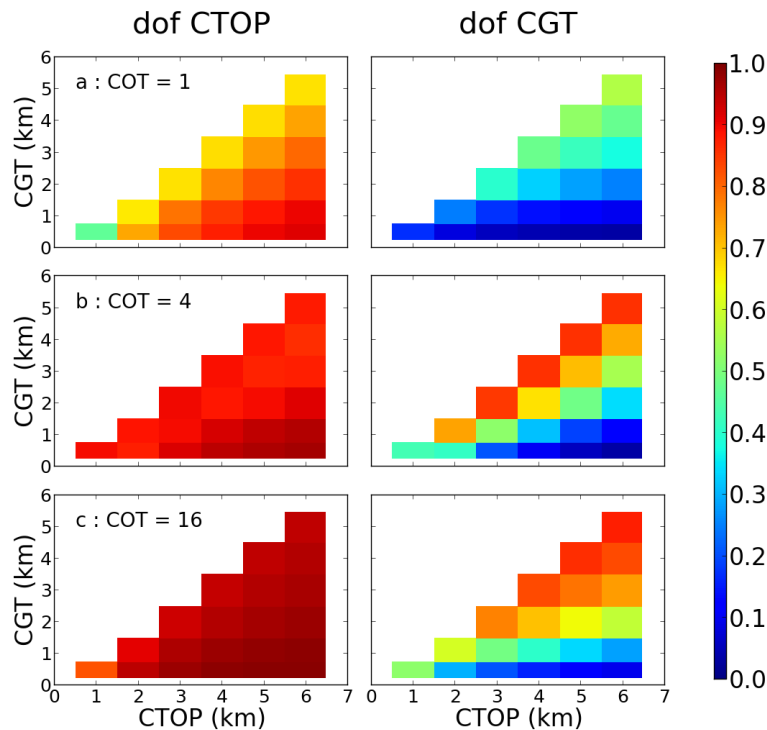


Figure 18. Same as Figs. 13 and 17 with an albedo of 0.8. There is an interesting increase in information content for the moderately opaque ($\text{COT} = 4$) clouds when they are relatively thick, say, $\text{CGT} \geq \max\{2, \text{CTOP} - 2\}$ km.